Peel, M., Cross, S., Birkholz, O., Aladag, A., Piehler, J., & Peel, S. (2015). Rupture of Stochastically Occurring Vesicle Clusters Limits Bilayer Formation on Alkane-PEG-Type Supports: Uncoupling Clustering from Surface Coverage. *Langmuir*, *31*(32), 8830-40. https://doi.org/10.1021/acs.langmuir.5b00925

Rupture of Stochastically Occurring Vesicle Clusters Limits Bilayer Formation on Alkane-PEG type Supports: Uncoupling Clustering from Surface Coverage

Journal:	*Langmuir*
Manuscript ID:	la-2015-009254.R2
Manuscript Type:	Article
Date Submitted by the Author:	n/a
Complete List of Authors:	Peel, Matthew; University of Bristol, Department of Mechanical Engineering Cross, Stephen; University of Bristol, School of Biochemistry Birkholz, Oliver; Universität Osnabrück, School of Biochemistry Aladag, Amine; University of Bristol, School of Biochemistry Piehler, Jacob; University of Osnabrueck, Department of Biology Peel, Suman; University of Bristol, School of Biochemistry

Rupture of Stochastically Occurring Vesicle Clusters Limits Bilayer Formation on Alkane-PEG type Supports: Uncoupling Clustering from Surface Coverage

*Matthew J. Peel, Stephen J. Cross, Oliver Birkholz, Amine Aladağ, Jacob Piehler and Suman Peel**

Dr. Stephen J. Cross, Dr. Amine Aladağ and Dr. Suman Peel

School of Biochemistry, University Walk, University of Bristol, Bristol, BS8 1TR, UK

E-mail: suman.peel@bristol.ac.uk

Dr. Matthew J. Peel

Department of Mechanical Engineering, University Walk, University of Bristol, Bristol, BS8 1TR, UK,

Oliver Birkholz and Prof. Dr. Jacob Piehler

Department of Biology, University of Osnabrück, Barbarastrasse 11, 49076 Osnabrück, Germany,

Keywords

Polymer-cushion supported bilayer, multi-vesicle assemblies, vesicle remodelling, super resolution imaging, multi-parameter surface-sensitive spectroscopy

Abstract

Polymer supported bilayers (PSBs) are a recognised tool for drug discovery through function-interaction analysis of membrane proteins. While silica supported bilayers (SSBs) spontaneously form from surface-adsorbed vesicles, successful PSB formation via a similar method has thus far been limited by insufficient understanding of the underlying vesicle-remodelling processes. Here, we generated a polymer support through incubation of poly-L-lysine conjugated to alkyl chain terminated poly(ethylene)glycol on silica. This polymer-coated silica substrate yielded efficient vesicle adsorption and spontaneous bilayer formation thereby providing a rare opportunity to address the mechanism of PSB formation and compare it to that of SSB. The combined use of super resolution imaging, kinetics and simulations, indicates the rupture of stochastically formed vesicle-clusters is the rate-limiting step, which is an order of magnitude higher for silica than polymer-coated silica. This was confirmed by directly demonstrating increased rupture-rates for surface adsorbed multi-vesicle assemblies formed by vesicle cross-linking in solution. Based on this key insight we surmised that a low propensity of cluster rupture can be compensated by an increase in number density of clusters: deposition of a mixture of oppositely charged vesicles resulted in bilayer formation on another alkane-PEG type of interface, which despite efficient vesicle adsorption, otherwise fails to support spontaneous bilayer formation. This potentially provides a universal strategy for promoting bilayer formation, on resistant surfaces without resorting to modification of the surface itself. Therefore, multi-vesicle assemblies with tailored geometries could not only facilitate bilayer formation on polymers with interesting functional properties but also instigate exploration of vesicle architecture for other processes involving vesicle-remodelling such as drug delivery.

Introduction

Silica supported bilayers (SSB) easily self-assemble[1, 2] and are amenable to a large number of analytical, imaging [3, 4, 5, 6, 7, 8, 9, 10] and fluidic tools.[11, 12] As a result they have served as model-membranes for studying varied fundamental cellular processes: interaction dynamics of cell surface receptors [10] and enzyme-catalysis [13] necessary for signal transduction; membrane fusion necessary for neurotransmission; [14] protein mobility and organisation necessary for cell to cell communication [15] and protein-membrane interaction necessary for membrane remodelling and fission. [16] In order to better mimic the cellular environment the use of soft polymer-spacers between bilayer and the substrate has been long advocated. [3, 17] However, with a few exceptions, [18, 19, 20, 21] bilayer formation by vesicle deposition on soft polymer interfaces has proven difficult to achieve as our limited understanding of the underlying vesicle remodelling processes required for bilayer formation prevents rational design approaches.

Through the use of bulk kinetics, it has been long recognised that the transformation of surface adsorbed vesicles into a bilayer occurs via multi-step vesicle remodelling processes. [22, 23, 24] Over the last decade membrane remodelling of substrate-bound giant and small uni-lamellar vesicles (GUV and SUV respectively) has been directly imaged by fluorescence microscopy, [25, 26, 27] atomic force microscopy (AFM) [28, 29, 30, 31, 32] and interferometric scattering microscopy.[9] This led to formulation of substrate-induced membrane remodelling paths that see surface-immobilised SUVs rupture or fuse (Scheme 1) *i.e.* (1) isolated vesicle rupture, [9, 25] (2) vesicle induced vesicle rupture, [9, 25] (3) vesicle-vesicle merger, [25] (4) bilayer edge induced vesicle rupture [9, 27, 33] and (5) bilayer-bilayer merger. [27] There is a lack of consensus regarding the relative contributions of these paths for SSB formation and due to a lack of polymers supporting spontaneous bilayer formation, contributions of these paths for PSB formation are completely unknown.

For SSB formation, the behaviour of exponential growth in vesicle rupture at a critical coverage was qualitatively captured in simulations by assuming an instantaneous rupture of clustered vesicles[34]. Bilayer patches so produced efficiently grew via bilayer-edge induced assimilation of vesicles while isolated vesicles were stable. In another study, simulations emulating an adsorption isotherm also suggested critical vesicle density to be important for vesicle-rupture[35]. Again, rupture was promoted by neighbouring vesicles (clusters) and was instantaneous if a

number threshold was met. The bilayer-patches were suggested to grow mainly by the targeted adsorption of vesicles to the bilayer-edge [35]; the efficiency of bilayer-edge-induced as well as spontaneous rupture of surface adsorbed vesicles was found to be low. [35] In contrast, label-free imaging of surface bound vesicles [9] suggested the rupture of isolated vesicles was the major source of bilayer-patches, with a critical vesicle density required to permit efficient spreading of the bilayer via bilayer-edge-induced vesicle (surface adsorbed) rupture rather than by vesicle-induced vesicle-rupture or vesicle–vesicle merger. Thus, the rate limiting step(s) during SSB formation remain contentious and any inhibitory impact on them by lipid composition, and crucially the support-type, is still sparse; rendering PSB formation by rational design highly challenging.

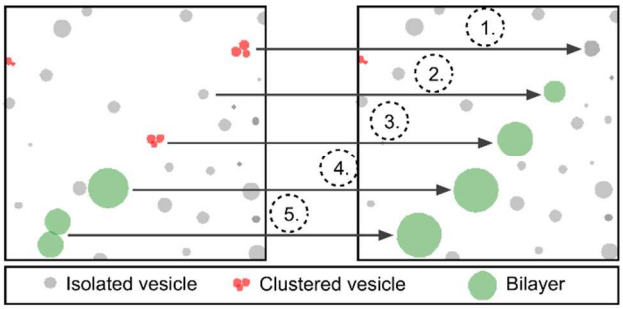

Scheme 1 Previously identified substrate-induced membrane remodelling pathways that see surface-immobilized SUVs rupture or fuse: (1) vesicle-vesicle merger, [25] (2) isolated vesicle rupture, [9, 25] (3) vesicle induced vesicle rupture, [9, 25] (4) bilayer edge induced vesicle rupture [9, 27, 33] and (5) bilayer-bilayer merger [27].

Here, we conjugated poly-L-lysine to alkyl chain terminated poly(ethylene)glycol. Polymer coated silica-substrate fortuitously supported efficient vesicle adsorption and spontaneous bilayer formation thereby providing a unique opportunity to address why bilayers readily form on silica substrate yet have considerable difficulty on soft polymers. We attempted to gain insight into SSB and PSB formation through the combined use of super resolution imaging, kinetics and simulations specifically designed to determine the rates of the different vesicle remodelling pathways (Scheme 1). This facilitated identification of the rate limiting step. We find bilayer-patch formation upon rupture of stochastically occurring vesicle clusters is the overall rate-limiting step on both the supports. However, this rate is an order of magnitude smaller on the

polymer support. The increased rupture rate of clustered vesicles is directly demonstrated by depositing pre-cross-linked vesicles. Furthermore, we show that using a mixture of oppositely-charged vesicles increases the propensity to form bilayers on a different alkane-PEG type of interface, which efficiently adsorbs vesicles but normally fails to support spontaneous bilayer formation. We surmise this occurs due to an increased number density of clusters on the surface and perhaps by increasing their rate of rupture. This result implies that a strategy of mixing oppositely-charged vesicles may provide a near-universal method for nucleating bilayer patches, thereby enabling continuous bilayer formation on soft-polymer surfaces. Notably, this method does not require an alteration of the surface simply to promote bilayer formation.

The results emphasise the role of multi-vesicle assemblies not only for PSB formation but potentially for other processes requiring vesicle-fusion such as drug delivery.

Experimental Section

We attempted to gain insight into SSB and PSB formation by developing a simulation specifically targeted at identifying the rate limiting steps. Our approach involved modelling vesicles and bilayers as explicit entities furnished with a rule set covering the pathways shown in Scheme 1. All but one path relies on the close proximity of multiple entities, the spatial distribution of vesicles as they are immobilised on the surface is therefore a key parameter and is determined experimentally using super-resolution fluorescence imaging. The simulation runs in a stepwise manner with the rate of each pathway recast as a probability of occurrence over the time scale of each step followed by calculation of experimentally accessible aggregate behaviour such as the fraction of intact vesicles and extent of membrane-merger as a function of time (Scheme 2). Experimental measurement of these i.e. fraction of intact vesicles and extent of membrane merger in conjunction with the amount of deposited vesicles (which serves as an input for the simulation) in real time was achieved simultaneously using a previously described system combining reflectance interferometry with total internal reflection fluorescence spectroscopy (RIF-TIRFS) and automated fluidic sample delivery. [10, 36] A direct comparison between measurements and simulations for the rates of vesicle rupture and membrane merger for partial and full coverage of the surface enabled determination of rate constants for different paths and identification of the rate-limiting steps for SSB and PSB formation for SUVs composed of 1-

stearoyl-2-oleoyl-*sn*-glycero-3-phosphocholine (SOPC).

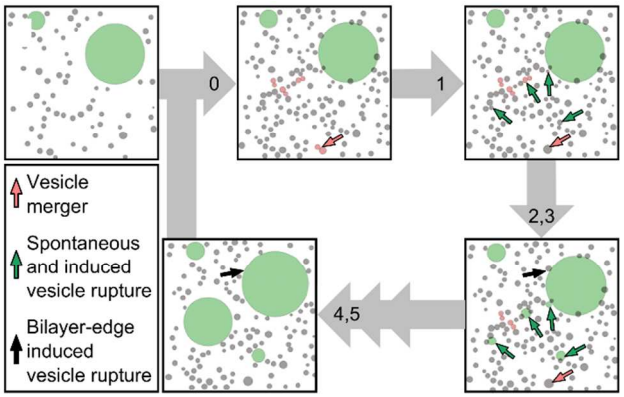

Scheme 2 Simulation stages: From an initial state (0) vesicles are deposited on the surface in accordance with the measured RIF trace at random locations outside the occluded area (*i.e.* not on top of a bilayer or a vesicle). (1) Vesicles in contact may merge with a probability P_M**.** (2,3) Vesicles have a chance to rupture into bilayers: isolated vesicles with a probability P_0; vesicles with N contacts with probability P_N. (4,5) Bilayer edge induced vesicle rupture is carried out with a probability P_R. Bilayer-bilayer merger always occurs to reflect the high reactivity of bilayer edges. The cycle is repeated every Δt (typically 100 ms). For a given input RIF time-trace and different values of P_M, P_0, P_N and P_R fluorescence traces for membrane merger and vesicle rupture are simulated and compared with the experimentally measured traces.

Simultaneous measurement of rate of vesicle adsorption, vesicle rupture and membrane merger

To correlate the rate and extent of vesicle deposition with vesicle rupture and membrane merger we employed a mixture of non-labelled SOPC SUVs , SUVs encapsulating RhoB and SUVs doped with 10 mol% of DHPE-OG488 such that the final vesicle proportions were 85:10:5 respectively. Changes in surface adsorbed mass and emission intensities for OG488 and RhoB were measured simultaneously in real time using reflectance interference (RIF) and total internal reflection fluorescence spectroscopy (TIRFS) in flow-through conditions using a home-built set-up described previously.[10, 36] Partial or full surface coverage was achieved by varying the total lipid concentration while maintaining a constant injection time.

Determination of spatial distribution of adsorbed vesicles through super resolution microscopy

and spatial point pattern analysis

Spatial distribution of adsorbing vesicles is a critical input for simulations. Therefore, SOPC SUVs doped with Sulforhodamine B conjugated to DHPE, were imaged using an objective-coupled TIRF microscopy configuration with a 561 nm laser, 150x objective lens (NA = 1.45; UAPON, Olympus) and scientific CMOS camera (2x binning, L_{px} = 6.5 μm; Orca Flash 4.0, Hamamatsu). Fluorescence of RhoB was excited in the evanescent field with high excitation intensity where all vesicles showed a fast drop in emission arising from photo-bleaching, thereby allowing recording of a large number of single-vesicle deposition events with high spatial precision. Each image was convolved with a Gaussian kernel of root mean square (RMS) width equal to 82 nm (corresponding to an estimated spread function (PSF) full width half maximum (FWHM) of 193 nm) to achieve low-pass filtering of noise [7–9]. Detection and fitting of vesicle PSF with sub-pixel accuracy is implemented in MATLAB and based upon the CLEAN algorithm of Högbom [37, 38] where user defined uniform intensity threshold was implemented as described before [38, 39] and instances of sub-diffraction limited localisation were discarded through filtering each PSF against a maximum width and ellipticity [40, 41, 42]. This led to a time stack with each frame containing coordinates for vesicles detected over multiple consecutive frames before they completely bleach. We needed to link these coordinates in time to obtain a unique vesicle map. Detected coordinates in a given frame were linked with the ones in the previous frame by identifying the minimum spatial separation between positions in adjacent frames (maximum 120 nm permitted) [43], with failure to identify a link followed by repetition at increasingly large temporal separations to a maximum of 5 seconds.

Vesicle coordinate maps so obtained were analysed for similarity to complete spatial randomness (CSR) using a normalised form of Ripley's K-function [44]; denoted *L(r)*, where, K(r) is the Ripley's K-function, $k_{i,j}$ takes a value of 1 if the inter-vesicle spacing ($r_{i,j}$) is less than or equal to *r* and a value of 0 otherwise. Edge-correction is applied with the $w_{i,j}$ term and has been described in detail elsewhere [45, 46].

$$L(r) = \sqrt{\frac{K(r)}{\pi}} = \sqrt{\frac{A}{\pi N^2} \sum_{i=1}^{N} \sum_{j=1.i\neq j}^{N} k_{i,j} w_{i,j}}$$

For distributions exhibiting CSR, this conversion yields zero *L(r)* for all lengths (r). Positive or

negative deviation of L(r) from 0 for any r demonstrate clustering or dispersion respectively at that length scale[47]. In order to account for a finite number of particles and area, a 99% L(r) confidence level was calculated by simulating 500 point patterns for each data set with comparable area and particles.

Simulating bilayer formation and calculation of vesicle rupture and membrane merger

A detailed description, underlying approximations, assumptions and their justifications, are presented in the supporting information. Briefly, the model operates in a sequential framework consisting of distinct phases within a discrete time step (Δt, generally < 100 ms). From an initial state (Scheme 2, step 0) an experimentally determined mass of vesicles is deposited on the surface such that vesicle do no deposit on an occluded area (*i.e.* not on top of a bilayer or a vesicle). Surface adsorbed vesicles are not allowed to laterally diffuse (Figure S1, Supporting Information). Some overlap (f_0) with surface bound vesicles is permitted; this indirectly determines how many vesicles may be in contact at a given surface coverage. The ensemble is then evolved according to known membrane remodelling pathways (Scheme 1) through different stages of simulation (Scheme 2). Vesicles in contact may merge with a probability $P_{M.}$ (Scheme 2, step 1). Vesicles have a chance to rupture into bilayers (Scheme 2, step 2,3): isolated vesicles with a probability P_0; vesicles with N contacts with a probability $\boldsymbol{P_N = P_0(1 + FN^C)}$, where F and C are parameters reflecting the strength of the clustering effect. Bilayer edge induced vesicle rupture is carried out with a probability P_R and bilayer-bilayer merger always occurs to reflect the high reactivity of bilayer edges (Scheme 2, step 4,5). Bilayers grow and change their boundaries during this process often creating new contacts. Each contact is tested once.

Probabilities of individual paths could be determined unambiguously with a complete knowledge of the number and spatial distributions of surface bound species as a function of time; however, direct experimental determination of these remains beyond current technological scope. For a given set of probabilities (rate constants), our simulation methodology allows estimation of experimentally accessible aggregate behaviour such as the fraction of intact vesicles and extent of membrane-merger as a function of time. For a given adsorption process (RIF trace) RhoB and OG488 traces can be simulated by (i) tracking the total internal volume of unmerged vesicles and (ii) from the weighted mass of labelled and unlabeled lipids according to the experimentally measured de-quenching curve (Figure S2, Supporting Information) and then integrated. A direct comparison between measurements and simulations for the rates of vesicle rupture and

membrane merger for partial and full coverage of the surface enabled determination of the rate constants.

Results and discussion

Vesicle-adsorption on silica is diffusion controlled and vesicle-distribution spatially random

In order to determine the relative contributions of different vesicle remodelling pathways for silica we simulated and experimentally measured the rate of vesicle adsorption, vesicle rupture and membrane merger by injection of a 85:10:5 mixture of label-free SOPC SUVs, SUVs encapsulating Sulphorhadmine B and SUVs doped with 10 mol% of DHPE-OG488 to achieve surface saturation (Figure 1). Here, RIF served as an absolute measure of mass where 4.4 ng/mm^2 is the surface coverage for a defect free contiguous bilayer composed of SOPC. [10, 36] Vesicle remodeling pathways 1-4 contribute towards a drop in RhoB signal through vesicle-content loss resulting from vesicle rupture. At 10 mol% OG488 is heavily quenched (Figure S2, Supporting Information); vesicle remodeling pathways 2-5 contribute towards a rise in OG488 signal through fluorescence de-quenching upon dilution as a result of membrane merger. It is noteworthy that in the absence of lipid mixing and vesicle rupture, RhoB and OG488 traces report on vesicle deposition alone and so should match the RIF trace.

As noted elsewhere,[29 22] vesicle deposition increases linearly till saturation (Figure 1, RIF trace) indicating the association process is diffusion controlled (further supporting data in Supporting Information, Figure S3), rather than driven by affinity to the surface or bilayer-edges [33, 35]. This linearity is maintained despite lipid mixing and vesicle rupture starting well before saturation, as evidenced by a sharp rise in OG488 trace and decline in RhoB trace at 2.2 ng/mm^2, suggesting creation of bilayer-edges had limited impact on vesicle adsorption. Lateral interactions such as vesicle-vesicle and vesicle-bilayer contacts, the numbers of which likely increase with surface loading, affect the rate of vesicle rupture and lipid mixing, thereby modulating the contribution of different vesicle remodelling pathways shown in Scheme 1. Under conditions of complete spatial randomness (CSR), a certain number of vesicles is expected to be in physical contact with other vesicles. Therefore, the degree of clustering will be a function of the number density of vesicles on the surface *i.e.* coverage. We can also speculate that the ability of a bilayer to grow will depend on the number of vesicles in the neighbourhood since low vesicle densities mean the bilayer edge will be unlikely to contact, and hence incorporate, a constant stream of vesicles as it grows. These inferences would be inaccurate if deposition deviates from CSR. Thus, correctly determining the degree of randomness, dispersion or clustering in the deposition process is critical in properly implementing the simulation. However, experimental determination of vesicle

distribution at sufficiently high loading for meaningful statistical analysis is non-trivial as (i) conventional fluorescence super-resolution methods don't apply and (ii) scanning probe microscopy risks being too invasive as tip mediated relocation of vesicles during scanning cannot be ruled out. As surface bound vesicles are essentially immobile (Figure S1, Supporting Information), we therefore used fluorescence super-resolution microscopy in conjunction with ongoing adsorption and rapid photobleaching.

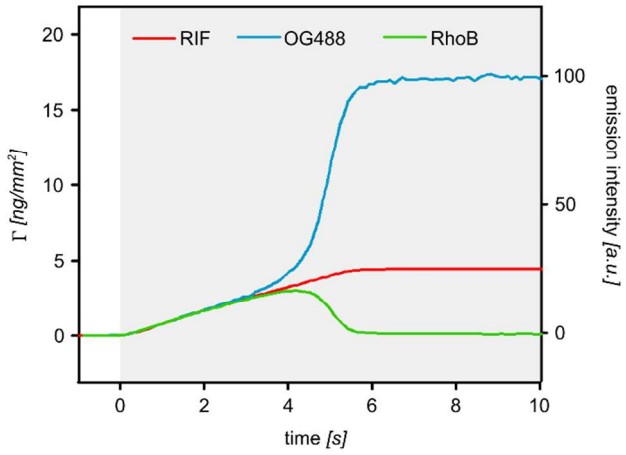

Figure 1 Vesicle binding to silica is diffusion rather than affinity controlled and vesicle rupture and membrane merger begins well before surface saturation: Simultaneous measurement of vesicle deposition (RIF trace, red), vesicle rupture (Oregon Green 488, blue) and membrane merger (Sulforhodamine, green). Injection period is marked with a grey background.

For determining the spatial distribution of depositing vesicles, we utilized SOPC SUVs doped with 0.1% sulforhodamine-DHPE and imaged the surface using objective coupled TIRFM. High photo-bleaching rates enabled recording of all single-vesicle deposition events with high spatial precision. Figure 2 A shows a typical frame and Figure 2 B shows the magnified crop for 4 consecutive frames demonstrating transient-detection of surface bound vesicles. For each full frame, centroids of the individual vesicles were determined by fitting a 2D Gaussian to the diffraction-limited intensity profile [37, 48] followed by frame-to-frame tracking till they bleached. A map of all individual vesicles was thus obtained with a median spatial precision of 3 nm, Figure 2 C shows such a map for all vesicles detected in the window from 5-20% of the total

surface coverage on silica. Figure D shows a random distribution for an equal number of vesicles, demonstrating no appreciable difference to the measured distribution. These maps allowed calculation of the distance of each vesicle to its nearest neighbour, the histogram of which is plotted in Figure 2 E and compared to a simulated random distribution shown in Figure 2 F. Qualitatively the two histograms appear very similar, further indicating a random distribution of particles. Figure 2 G shows a comparison of a measured vesicle distribution (also in the range 5-20% of total surface loading) to CSR using Ripley's K-function test. [44] Deviation of the measured profiles outside the 99% confidence interval (black lines; generated from 500 simulations of random distributions) would indicate a departure from randomness at that length scale. Retention of the measured curves within the 99% confidence level implies random distribution of deposited vesicles.

Taken together, under our conditions vesicles do not preferentially associate with the bilayer-edges and appear to bind to the surface in a spatially random manner. Therefore, for determining the rate constants for different paths shown in Scheme 1, we used a CSR vesicle distribution and simulated the fluorescence traces by treating the RIF trace as a mass input. Since, as several pathways contribute to each fluorescence trace, as per our simulation methodology, rate constants for different paths (Scheme 1) could not be uncorrelated for a single surface coverage (Figure 1). As explained below these correlations can be countered by a strategy of multiple surface coverages and a global simulation that must satisfy all measurements.

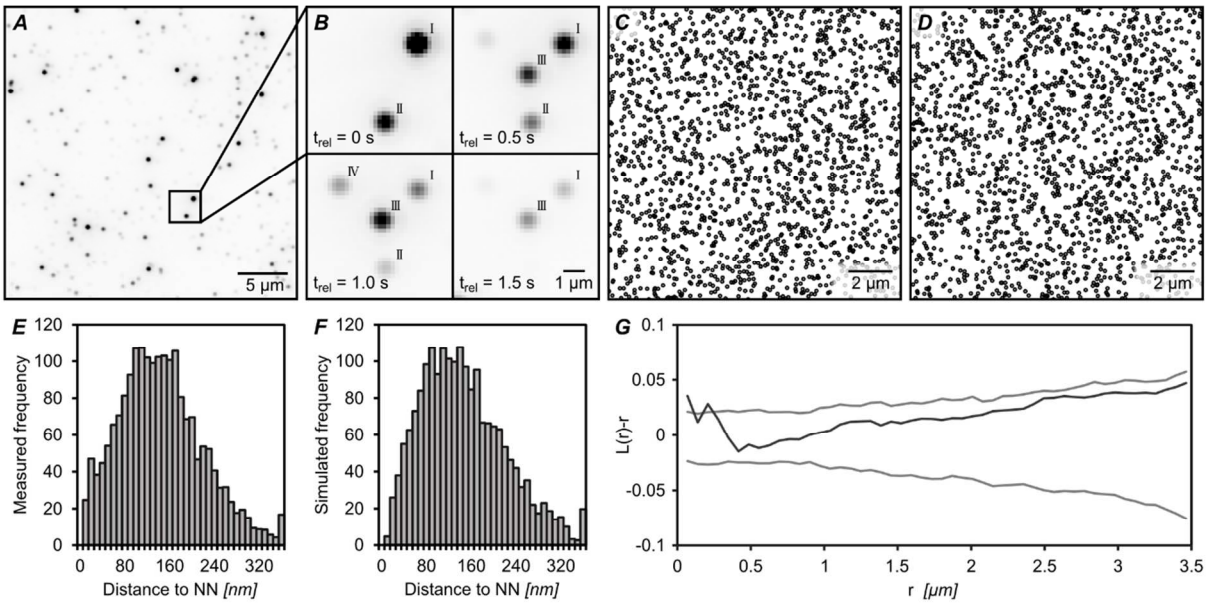

Figure 2: Super-resolution imaging shows random spatial distribution of surface bound vesicles: (A) A typical frame acquired using an objective coupled TIRFM with high laser power to ensure rapid photo bleaching. (B) 4 successive frames of the cropped area showing photo bleaching of the adhered vesicles and arrival of fresh vesicles. (C) Example location map of all vesicles deposited between 5-20% of full surface loading and (D) simulated random distribution for the same number of vesicles. Histograms showing distance of each vesicle to its nearest neighbour for (E) a measured vesicle location map, and (F) a simulated random distribution. (G) Comparison of measured vesicle distribution for the range of 5-20% of full surface loading (black line) to complete spatial randomness (CSR) using Ripley's K-function test. No deviation of the measured profiles outside the 99% confidence interval (generated from 500 simulations of random distributions; grey lines) indicates randomness at that length scale.

Rupture of stochastically occurring vesicle clusters is rate limiting for SSB and PSB formation

Variations in surface coverage lead to different spatial and number distributions of the reactant species (isolated vesicles, clustered vesicles and bilayer-edges) thus altering the relative contributions of each pathway. We took advantage of this feature by restricting the maximum surface coverage to fractions of a full bilayer and measuring the lateral processes, i.e. vesicle rupture and membrane merger, post-injection where surface coverage is unchanging. The use of RIF trace as a mass input during and post injection was therefore critically important. Comparing simulations with experiments for different surface coverage thus constrained the rates and reduced correlations. Short injection durations and variable lipid concentrations were used to

achieve variable surface loadings for measurement of vesicle rupture and membrane merger during and post injection. During the injection phase increase in mass with three different rates is a result of stop of flow followed by fast flushing of the dead-volume necessary for automating fluidic control (Figure 3, RIF traces). Figure 3 shows the experimental and simulated fluorescence traces for five different RIF traces showing maximum surface coverage of 0.46, 1.13, 2.37, 3.18 and 4.4 ng/mm^2. Simulated lateral distributions of isolated vesicles (grey circle), clustered vesicles (red circles) and bilayer patches (green circles) corresponding to each set of traces at three different time-points (during and post injection) is shown to the right (Figure 3). The rate constants determined by matching the simulations with experiments are summarized in Table 1. We find that the isolated vesicles are extremely stable ($k_{isolated} \leq 10^{-5}$ s^{-1}) but rupture much more readily when in contact with other vesicles. Bilayer edge-induced vesicle rupture is extremely rapid (≥ 100 s^{-1}) but accurate determination is limited by the data acquisition rate (10 Hz). Given the reaction rates and the relative abundance of isolated and clustered vesicles and bilayer patches (Figure 3, right panels), this analysis reveals that rupture of binary and higher clusters is the major driving force for nucleation of bilayer patches. Subsequently, these drive bilayer formation by bilayer-edge catalysis so long there are neighbouring vesicles available for further rupture.

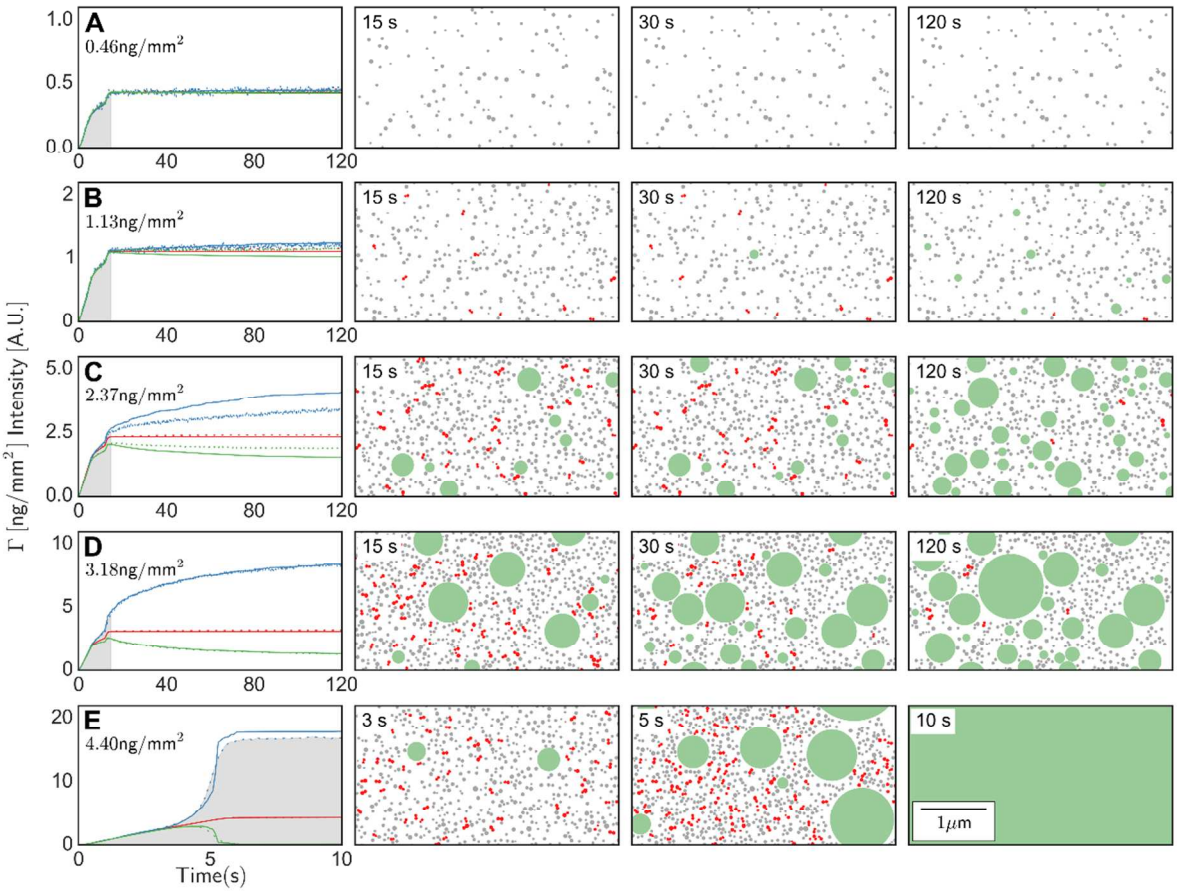

Figure 3 Measurements and simulations of surface loading dependent vesicle rupture and lipid mixing show rupture of clustered vesicles is the rate limiting step for SSB formation: Measured (dashed) and simulated (solid) RIF (red), RhoB (green) and OG488 (blue) traces for surface loadings of (A) 0.46, (B) 1.13, (C) 2.37, (D) 3.18, and (E) 4.4 ng.mm^{-2}. Injection period is marked with a grey background. Images to the right show the simulated spatial distribution of isolated vesicles (grey), vesicles in contact with other vesicles (red) and bilayers (green) at different time points for the corresponding simulated fluorescence traces.

These conclusions are qualitatively similar to Zhdanov *et. al.* with one key difference: in their case the probability of rupture of a cluster is fixed at 1. This assumption is incompatible with our observation of continued rupture of vesicles post-injection at low surface coverages. If clusters rupture as soon as they form, for a random distribution of vesicles, the number of nucleation sites is simply dictated by surface coverage and some chosen definition of contact distance. While this strategy captures the qualitative behaviour of exponential growth in vesicle rupture starting at a

critical coverage, it is impossible to infer anything about the underlying vesicle rupture behaviour. For example, should rupture of clustered vesicles be the differentiating factor between support types that behaviour will be lost. At the same time, the complete stability of vesicles at very low coverages (essentially no clusters) and the exponential growth of bilayers at high coverage limit the options for altering other remodelling pathways to compensate for flexibility in the cluster rupture rate. The approach of allowing remodelling rates to be free variables, rather than arbitrarily assigned values, but constraining the possible outcomes by global simulation of multiple surface coverages could be critical in establishing the differences between different surface types. In addition, this approach permits a clarification of the role of surface coverage which has been central to the discussion of bilayer formation for over a decade. Arguably, there are two major interpretations of the importance of surface coverage: (1) a critical vesicle coverage is essential for generating the required number of vesicle clusters which rupture with infinite efficiency. (2) While individual isolated vesicles efficiently rupture on their own, an increase in vesicle coverage helps efficient propagation of a bilayer through bilayer-edge induced assimilation of vesicles [9]. Our approach appears able to discriminate between the various proposed remodelling pathways and provides meaningful kinetic rate constants, which are expected to differ for different substrate types.

Table 1: Reaction rate constants for vesicle remodelling paths and their best estimates for SSB and PSB formation

Pathway	Rate equation	SSB $[10^{-5}.s^{-1}]$	PSB $[10^{-5}.s^{-1}]$
Isolated vesicle rupture rate	$k_{isolated} = \frac{1}{\Delta t} ln(1 - P_0)$	≤ 1	≤ 1
Binary cluster rupture rate	$k_{binary} = \frac{1}{\Delta t} ln(1 - P_1)$	421	38
Ternary cluster rupture rate	$k_{ternary} = \frac{1}{\Delta t} ln(1 - P_2)$	3361	75
Vesicle merger rate	$k_{merger} = \frac{1}{\Delta t} ln(1 - P_M)$	82.5	10
Bilayer-edge induced vesicle-rupture rate	$k_{bilayer} = \frac{1}{\Delta t} ln(1 - P_R)$	≥ 10^7	8.10^5

A further test for the methodology employed above would be to perform a similar analysis on a more complex substrate expected to alter some of the pathways. A high density of alkyl chains (AC) is known to promote vesicle adhesion[49] and polyethylene(glycol) has been shown to be a biocompatible non-interacting spacer-polymer.[49, 50, 51] For bilayer formation these properties have been successfully exploited by depositing AC terminated PEG (PEG-AC) on silica either covalently[18, 19] or with the aid of poly-l-lysine (PLL-PEG-AC).[20] However, bilayer formation could only be achieved upon prolonged incubation with soluble PEG.[18, 19 20] Here, we synthesized a new variant of PLL-PEG-AC (Figure 4 A-C). Silica coated with the polymer fortuitously yielded a bilayer upon vesicle deposition as indicated by full fluorescence recovery upon photo-bleaching (Figure 4 E): a diffusion coefficient (D) of 2.27 ± 0.30 $\mu m^2 s^{-1}$ and a mobile fraction of 1.02 ± 0.008 were obtained (experimental details in Supporting Information). This is comparable to a diffusion coefficient of 1.77 ± 0.09 $\mu m^2 s^{-1}$ and a mobile fraction of 1.08 for silica (Figure 4 E, blue line). This system provided us with a unique opportunity for understanding how lipid bilayers self-assemble on an alkane-PEG type of polymer.

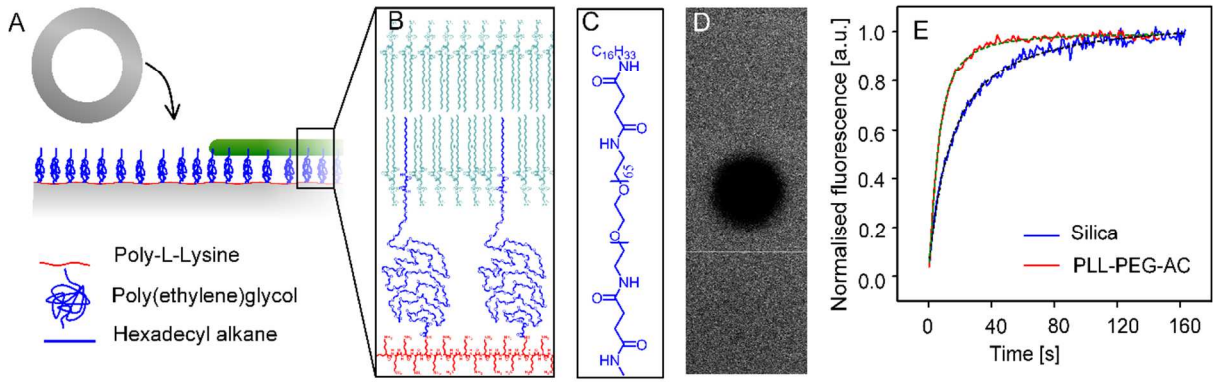

Figure 4 Vesicle deposition on PLL-PEG-AC leads to bilayer formation: (A) Surface architecture of silica coated with PLL-PEG-AC. (B) Chemical architecture of PLL-PEG-AC and SOPC bilayer (C) Chemical structure of PEG-AC attached to PLL. (D) Confocal laser scanning images showing fluorescence-recovery after photo-bleaching for a bilayer formed by SOPC vesicle doped with 0.2% OG488-DHPE on PLL-PEG-AC; first frame: immediately before photo-bleaching, second frame: immediately after photobleaching, third frame: 30 s post bleaching. (E) Normalised fluorescence from the bleached region demonstrating efficient recovery over time for silica (blue line) and PLL-PEG-AC (red line).

While overall deposition, vesicle rupture and membrane merger behaviour is similar to silica (Figure S4), SUV deposition occurs at a reduced rate (Figure S3 B) Deviation of fluorescence traces from the RIF trace start at higher surface loading (3.45 ng/mm^2, Figure 5E) compared to the silica surface (2.2 ng/mm^2) implying a general increase in vesicle stability. Figure 5 shows the experimental and simulated RIF and fluorescence traces for the surface coverages 0.41, 3.45, 3.66, 3.89 and 4.40 ng/mm^2. The best determined kinetic constants for vesicle remodelling pathways are listed in Table 1. As with silica, spontaneous vesicle rupture is very slow and vesicles are strongly destabilized by contact with a partner (vesicle or bilayer). However, vesicles are less prone to rupture and merger on PLL-PEG-AC than on silica e.g. rupture of binary clusters, vesicle-vesicle merger and membrane edge induced vesicle rupture are all nearly an order of magnitude slower on PLL-PEG-AC than on silica. This point is best illustrated by the simulated spatial distribution of the surface bound entities which is shown to the right of the traces at three different times. For similar surface loadings, considerably larger amounts of clustered vesicles are visible on PLL-PEG as compared to silica (Figure 5 B and 3 D respectively).

Higher vesicle stability on a polymer cushion may result from several reasons. On a hard interface like silica, vesicle adhesion is likely to be accompanied by distortion and high local curvature thus making them prone to rupture (Scheme 3). In comparison, a softer support with conformational flexibility of the polymer may prevent excessive vesicle distortion leading to decreased rupture rate. It proved difficult to demonstrate this effect for isolated vesicles as due to experimental constrains only a lower limit of 10^{-5}. s^{-1} on rupture of isolated vesicles could be determined. As opposed to isolated vesicles, a clear difference in incorporation of surface adsorbed vesicles into existing bilayer patches was observed. This process was an order of magnitude slower on PLL-PEG-AC as compared to silica (Table 1 and Scheme 3). This could result either from minimal distortion of vesicles and/or less reactive bilayer-edges. Sequestration of the polymer attached alkyl chains may help stabilise the otherwise exceedingly reactive bilayer edges. Merger and rupture of clustered vesicles exhibited a similar trend. For binary clusters the rupture rate on silica was an order of magnitude higher than on PLL-PEG-AC. We attribute this difference to substrate induced vesicle distortion (Scheme 3). Vesicles exhibiting high membrane curvature, arising from increased substrate contact area, are more likely to undergo membrane-merger leading to either leaky vesicle-fusion or rupture.

Taken together, efficiency of different vesicle remodelling pathways was found to be different for PLL-PEG-AC and silica. Surprisingly, despite such different surface types, rupture of clustered vesicles still proved to be the rate-limiting step for PLL-PEG-AC as was the case for silica.

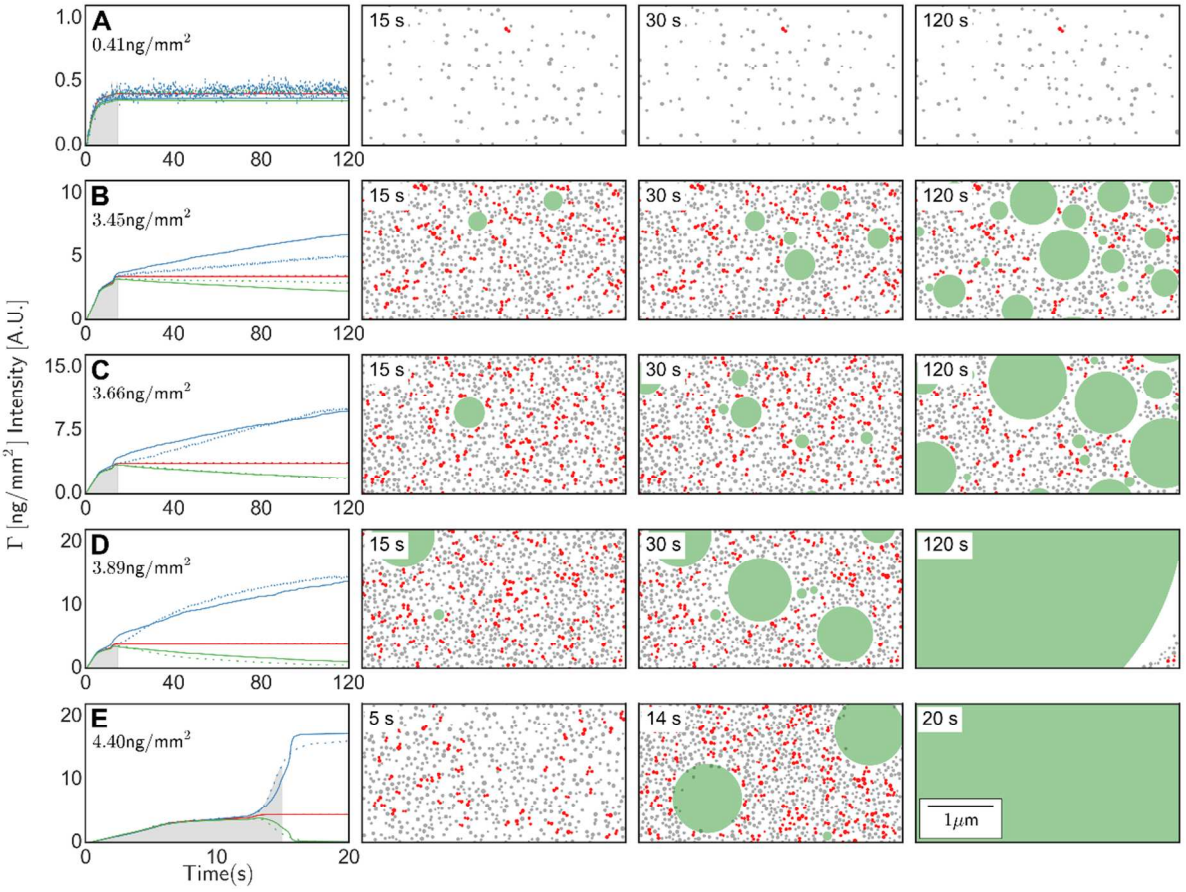

Figure 5 Measurements and simulations of surface loading dependent vesicle rupture and lipid mixing show rupture of clustered vesicles is the rate limiting step for PSB formation: Measured (dashed) and simulated (solid) traces for RIF (red), RhoB (green) and OG488 (blue) for surface loadings of (A) 0.41, (B) 3.45, (C) 3.66, (D) 3.89, and (E) 4.4 ng.mm^{-2}. Injection period is marked with a grey background. Images to the right show the spatial distribution of isolated vesicles (grey), vesicles in contact with other vesicles (red) and bilayers (green) at different time points. Scale bar 1μm.

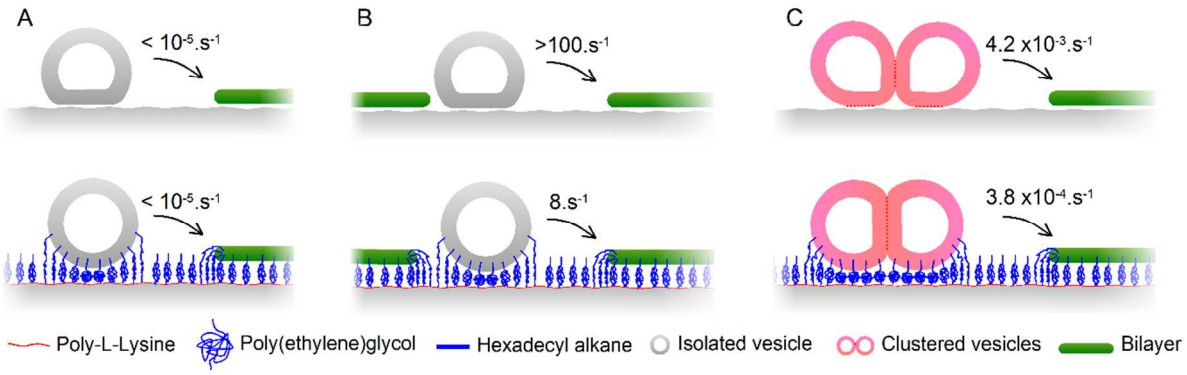

Scheme 3 Rate constants for a selection of vesicle remodelling paths on silica and silica coated with PLL-PEG-AC: A) rupture of individual vesicles to form isolated bilayer patches, B) Bilayer-edge induced assimilation of vesicles, C) rupture of binary vesicle cluster to form an isolated bilayer patch.

Increased reactivity of vesicle clusters

Allowing clustered vesicles, as compared to single isolated ones, a greatly increased rate of rupture was critical in matching the simulation to the measured traces. Therefore, for a direct experimental verification of this prediction we attempted to measure the rupture rate of vesicles cross-linked with streptavidin. Upon crosslinking vesicles demonstrated a near doubling of their hydrodynamic diameter, however in the absence of scattering cross-sections for single, binary and further clusters it proved difficult to determine their relative proportions (Supporting Information, Figure S5). Cross-linked and uncross-linked vesicles were injected on silica and PLL-PEG-AC such that surface loadings were < 0.8 ng/mm^2 – well under the threshold where uncrosslinked SUVs show loss of encapsulated dye. As the deposited vesicles do no dissociate from the surface (Supporting Information Figure S6), a decay in fluorescence can only be attributed to vesicles being destabilized by the substrate. Shown in Figure 6 are the normalized RhoB TIRFS traces for vesicles with and without cross-linking. On silica, as expected, un-cross-linked vesicles exhibit no drop in RhoB trace during the washing phase whereas cross-linked vesicles demonstrate a significant decay. Similarly, PLL-PEG-AC cross-linked vesicles showed a smaller but significant decay. Interestingly, on a previously reported interface (PEG-AC linker (Figure 4 C) coupled covalently to the silica surface silanised with 3-Glycidyloxypropyl)trimethoxysilane)[18] where bilayer formation by vesicle deposition could only be achieved upon prolonged incubation with soluble PEG, cross-linked vesicles did not exhibit any dye loss (Figure 6 C). Presumably the substrate offers further vesicle stabilization to that

provided by both silica and PLL-PEG-AC; this is further evidenced by the lack of spontaneous bilayer formation on this substrate. It appears that crosslinked vesicles are indeed less stable than isolated individual vesicles albeit to a different extent depending upon the nature of the polymer cushion.

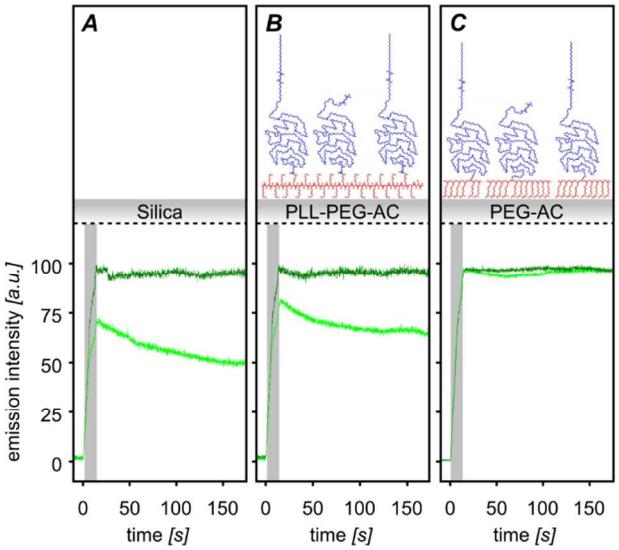

Figure 6 Increased rupture rates of pre-clustered vesicles: Normalized RhoB trace for cross-linked (light green) and un-cross-linked (dark green) vesicles on (A) silica, (B) PLL-PEG-AC and (C) PEG-AC.[18] Injection periods are marked with a grey background. Top panels show the surface-types.

Promoting bilayer formation on polymer cushions: Uncoupling clustering from surface coverage

While crosslinking with streptavidin proved useful in demonstrating increased rupture propensity for vesicle clusters, such undefined protein-mediated clusters as nucleation sites are suboptimal and are not a universal solution for inducing bilayer formation. Nonetheless, this analysis helped us consolidate the central role of clusters and formulate a summary of what we think are the necessary requirements for a defect free continuous bilayer formation on polymer cushions,

(1) Sufficient surface coverage: So long a surface allows for adsorption of ~ 4.4ng/mm^2, in principle, efficient propagation of bilayer patches through bilayer-edge assimilation of vesicles and complete coverage of the surface can be achieved. While this is readily achieved for silica and mica type surface, ultrathin, hydrophilic, noncharged polymers such as carbohydrates or poly(ethylene glycol) (PEG) which are typically used for biotechnological applications show

minimal adsorption of vesicles[17, 52, 53, 54, 55, 56, 57, 58]. This problem is solved by incorporating alkyl chains at polymer terminus as efficient anchors for vesicles[59]. Alkane-PEG type of architectures have proven to be particularly successful in ensuring this requirement[18, 19, 20].

(2) Favourable lateral distribution: Lateral distribution of the adsorbed vesicles must allow for some clustering to occur. Dispersed and clustered distribution are therefore expected to hinder and promote bilayer formation as compared to a random distributions. Therefore, vesicles composed of charged lipids, due to electrostatic repulsion, could show a dispersed distribution hence poor propensity for bilayer formation. Adsorption hot spots arising from surface heterogeneity could be another factor in determining the lateral distribution.

(3) Efficient rupture of clusters: Clustered vesicles display differential propensity of rupture on different surface types, silica > PLL-PEG-AC > PEG-AC. Evidently, hard interfaces appear to be more efficient than soft polymer cushions. Given the lack of available data on rupture of vesicle clusters it is difficult to predict how different polymer surface types can alter the propensity for vesicle rupture. Equally, customising the polymer to aid vesicle rupture may conflict with other requirements for the surface (e.g. biocompatibility).

Our model suggests that for nucleation of bilayer patches a low probability of rupture can be compensated by increasing the number density of clusters. Alternatively, the effect of a high propensity for rupture could be diminished via a dispersed distribution. As discussed above, PLL-PEG-AC is positively charged and supports efficient adsorption of neutral vesicles (SOPC), which then form a bilayer. Negatively charged vesicles are likely to efficiently deposit and strongly adhere to the surface but mutual repulsion will reduce the propensity to cluster. Therefore, despite allowing for full surface coverage, negatively charged vesicles may fail to produce a bilayer. We tested this hypothesis by performing a FRAP measurement with SOPC vesicles doped with 20% DOPS, 0.2 % OG488 DHPE (overall negatively charged). In contrast to neutral vesicles (SOPC), which exhibits a diffusion coefficient (D) of 2.27 ± 0.30 $\mu m^2 s^{-1}$ and a mobile fraction of 1.02, negatively charged vesicles exhibited next to no florescence recovery. This suggests an impact of electrostatics on clustering of vesicles and prompted us to further test the potential of electrostatics on bilayer formation. Surfaces exhibiting high propensity for vesicle adsorption but low propensity for rupture of clustered vesicles would form a good test substrates e.g. PEG-AC. We reasoned that a mixture of negatively and positively charged vesicles may lead to vesicle-vesicle interaction in solution and a clustered vesicle distribution on

a surface. A 1:1 mixture of negatively charged (20% DOPS, 80% SOPC) positively charged (20% DOTAP, 80%SOPC) vesicles exhibited increased scattering upon mixing in solution (Figure S7 Supporting Information) indicating vesicle-vesicle interaction in solution. We therefore incubated PEG-AC with neutral (SOPC), negatively charged (20% DOPS, 80% SOPC), positively charged (20% DOTAP, 80%SOPC) and 1:1 mixture of oppositely charged vesicles. In order to test for altered FRAP behaviour resulting from vesicles potentially perfused in solution we also incubated the surface with vesicles composed of mixed oppositely charged lipids (10% DOPS, 10% DOTAO, 80% SOPC). Following an incubation for 30 minutes, the FRAP measurements for each condition is shown in Figure 7. All four case of a single type of vesicle failed to show any fluorescence recovery after photo-bleaching indicating a lack of a contiguous bilayer. Conversely, a 1:1 mixture of oppositely charged vesicles showed a bilayer with a diffusion coefficient of $2.25 \pm 0.029\ \mu m^2.s^{-1}$ and recovered fraction of 1.01 ± 0.001. It seems likely that the primary driver for this change in behaviour is the increased number density of clusters, although we cannot rule out the possibility of tighter binding of vesicles of opposite charge leading to a higher propensity of cluster rupture. In either case, the net effect is to encourage bilayer formation on a difficult surface without requiring any change to the surface and with only minimal impact on bilayer composition.

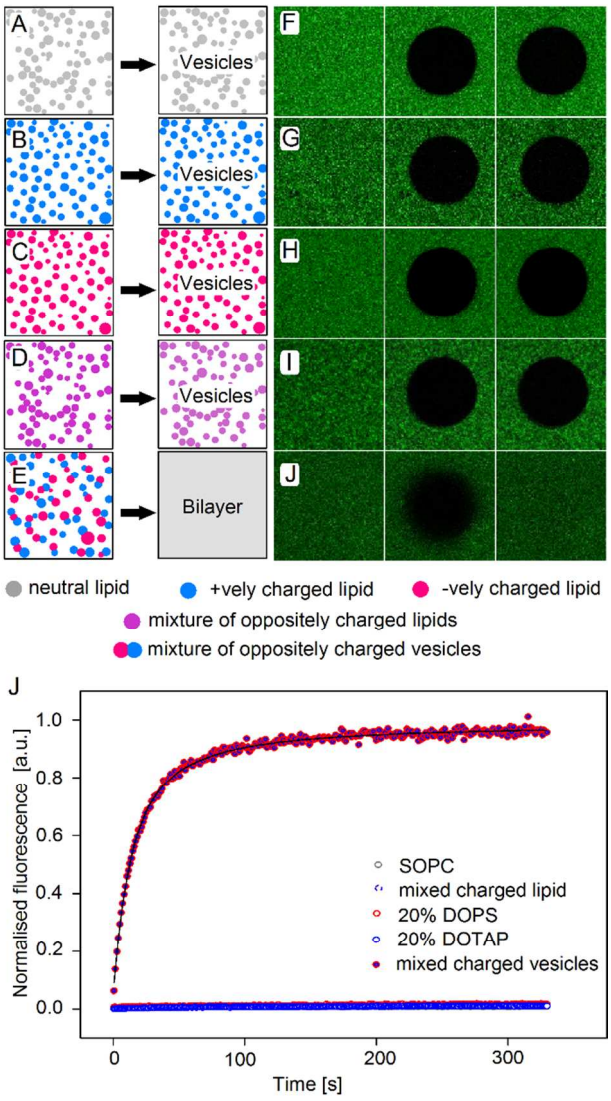

Figure 7 Promoting bilayer formation via electrostatically induced clustering: Schematic representation of lateral distribution of (A) neutral, (B) positively, (C) negatively and (D) a mixture of positively and negatively charged lipids and (E) a mixture of positively and negatively charged vesicles on a neutral PEG-AC surface. Frames before bleaching, immediately after bleaching and 30 s post bleaching for surface adsorbed (F) SOPC, (G) 20% DOPS+ 80% SOPC, (H) 20% DOTAP + 80% SOPC (I) 10% DOTAP + 10% DOPS + 80% SOPC and a (J) 1:1 mixture of 20% DOPS and 20% DOTAP vesicles. (K) Intergrated fluorescence from the bleached spot as a function time for SOPC (black open circle), 20% DOPS+ 80% SOPC (red open circle), 20% DOTAP + 80% SOPC (blue open circle), 10% DOTAP + 10% DOPS + 80% SOPC (red and blue open circle) and a 1:1 mixture of 20% DOPS and 20% DOTAP vesicles (red and blue circle).

For using clustered vesicles as nucleators for generation of bilayer patches, several further optimisations can be envisioned such that overall lipid composition of the bilayer is minimally impacted. A number of factors could have an impact on efficiency of cluster formation and stability of the cluster. We think the common point of contact between the substrate and the vesicles is where the membrane remodelling process begins. Therefore line tension generated through phase separation within vesicles forming a cluster could have a significant impact on the stability of the cluster. Taken together a combination of two or more of the following strategies could produce highly potent clusters: (i) Vesicle crosslinking via complementary DNA strands for stoichiometrically better defined cluster; (ii) Oppositely charged vesicles with optimised doping of charged lipids and proportions of charged vesicles; (iii) Phase separation within individual vesicles forming a cluster.

Conclusion

Over the last decade the mechanism of SSB and PSB formation has been extensively studied and several alternative mechanisms have been proposed. However, the rate constants for different steps remained undetermined. We have combined super-resolution imaging with the measurement and global simulation of the kinetics of vesicle rupture and membrane merger. Multiple surface coverages has allowed us to determine differential contributions of several previously proposed vesicle remodelling pathways. In contrast to previous studies, where an infinite efficiency of rupture clustered vesicles is assumed, we find the efficiency to be very modest. Bilayer nucleation is further limited by the number density of vesicle clusters. A simple cross-linking strategy helped differentiate vesicle rupture rates in a substrate dependent manner, thus demonstrating the importance of multi-vesicle assemblies for processes involving vesicle remodelling. Improving cluster density by mixing oppositely charged vesicles had an even more potent effect and permitted bilayer formation on PEG-AC which otherwise fails to produce a bilayer. While the efficiency of vesicle rupture may be difficult to alter, our results suggest the number density of clusters may be increased, thus forming a bilayer without resorting to modifications of the surface itself.

It is likely that more sophisticated crosslinking approaches capable of producing geometrically defined multi-vesicle assemblies would have greater success and so not only promote the use of polymers with interesting functional properties that better mimic varied cellular membrane

architectures but also as potential vehicles for drug delivery to cellular membranes.

Acknowledgements

The support from the laboratory of H. Hörber is gratefully acknowledged. We also thank R. Kurre for his support with super-resolution imaging, C. You for experiments demonstrating vesicle crosslinking, M. Bhagawati and A. Lawrie for many helpful discussions. This work was supported by an ERC starting grant.

Supporting Information Available: Figures S1–S7 as described in the text and further materials and methods are available. This information is available free of charge via the Internet at http://pubs.acs.org/.

References

(1) Brian, A. A.; McConnell, H. M. Allogenic stimulation of cyto-toxic T-cells by supported planar membranes. *Proc Natl Acad Sci U S A* **1984,** *81*, 6159-6163.

(2) Tamm, L. K.; McConnell, H. M. Supported phospholipid bilayers. *Biophysical Journal* **1985,** *47*, 105-113.

(3) Heyse, S.; Stora, T.; Schmid, E.; Lakey, J. H.; Vogel, H. Emerging techniques for investigating molecular interactions at lipid membranes. *Biochim Biophys Acta* **1998,** *1376*, 319-338.

(4) Janshoff, A.; Steinem, C. Scanning force microscopy of artificial membranes. *Chembiochem : a European journal of chemical biology* **2001,** *2*, 798-808.

(5) Cooper, M. A. Advances in membrane receptor screening and analysis. *Journal of Molecular Recognition* **2004,** *17*, 286-315.

(6) Kiessling, V.; Crane, J. M.; Tamm, L. K. Transbilayer effects of raft-like lipid domains in asymmetric planar bilayers measured by single molecule tracking. *Biophysical Journal* **2006,** *91*,

3313-3326.

(7) Fox, C. B.; Wayment, J. R.; Myers, G. A.; Endicott, S. K.; Harris, J. M. Single-Molecule Fluorescence Imaging of Peptide Binding to Supported Lipid Bilayers. *Analytical Chemistry* **2009,** *81*, 5130-5138.

(8) Thompson, N. L.; Wang, X.; Navaratnarajah, P. Total internal reflection with fluorescence correlation spectroscopy: Applications to substrate-supported planar membranes. *Journal of Structural Biology* **2009,** *168*, 95-106.

(9) Andrecka, J.; Spillane, K. M.; Ortega-Arroyo, J.; Kukura, P. Direct observation and control of supported lipid bilayer formation with interferometric scattering microscopy. *ACS Nano* **2013,** *7*, 10662-10670.

(10) Gavutis, M.; Lata, S.; Lamken, P.; Muller, P.; Piehler, J. Lateral ligand-receptor interactions on membranes probed by simultaneous fluorescence-interference detection. *Biophys J* **2005,** *88*, 4289-302.

(11) Kelety, B.; Diekert, K.; Tobien, J.; Watzke, N.; Doerner, W.; Obrdlik, P.; Fendler, K. Transporter assays using solid supported membranes: A novel screening platform for drug discovery. *Assay and Drug Development Technologies* **2006,** *4*, 575-582.

(12) Jung, H.; Robison, A. D.; Cremer, P. S. Multivalent ligand-receptor binding on supported lipid bilayers. *Journal of Structural Biology* **2009,** *168*, 90-94.

(13) Iversen, L.; Tu, H. L.; Lin, W. C.; Christensen, S. M.; Abel, S. M.; Iwig, J.; Wu, H. J.; Gureasko, J.; Rhodes, C.; Petit, R. S.; Hansen, S. D.; Thill, P.; Yu, C. H.; Stamou, D.; Chakraborty, A. K.; Kuriyan, J.; Groves, J. T. Ras activation by SOS: Allosteric regulation by altered fluctuation dynamics. *Science* **2014,** *345*, 50-4.

(14) Domanska, M. K.; Kiessling, V.; Stein, A.; Fasshauer, D.; Tamm, L. K. Single vesicle

millisecond fusion kinetics reveals number of SNARE complexes optimal for fast SNARE-mediated membrane fusion. *The Journal of biological chemistry* **2009,** *284*, 32158-32166.

(15) Hartman, N. C.; Nye, J. A.; Groves, J. T. Cluster size regulates protein sorting in the immunological synapse. *Proc Natl Acad Sci U S A* **2009,** *106*, 12729-12734.

(16) Lata, S.; Schoehn, G.; Jain, A.; Pires, R.; Piehler, J.; Gottlinger, H. G.; Weissenhorn, W. Helical structures of ESCRT-III are disassembled by VPS4. *Science* **2008,** *321*, 1354-7.

(17) Tanaka, M.; Sackmann, E. Polymer-supported membranes as models of the cell surface. *Nature* **2005,** *437*, 656-663.

(18) Roder, F.; Waichman, S.; Paterok, D.; Schubert, R.; Richter, C.; Liedberg, B.; Piehler, J. Reconstitution of membrane proteins into polymer-supported membranes for probing diffusion and interactions by single molecule techniques. *Anal Chem* **2011,** *83*, 6792-6799.

(19) Waichman, S.; Roder, F.; Richter, C. P.; Birkholz, O.; Piehler, J. Diffusion and interaction dynamics of individual membrane protein complexes confined in micropatterned polymer-supported membranes. *Small* **2013,** *9*, 570-577.

(20) Ye, Q.; Konradi, R.; Textor, M.; Reimhult, E. Liposomes tethered to omega-functional PEG brushes and induced formation of PEG brush supported planar lipid bilayers. *Langmuir : the ACS journal of surfaces and colloids* **2009,** *25*, 13534-13539.

(21) Basit, H.; Van der Heyden, A.; Gondran, C.; Nysten, B.; Dumy, P.; Labbe, P. Tethered bilayer lipid membranes on mixed self-assembled monolayers of a novel anchoring thiol: impact of the anchoring thiol density on bilayer formation. *Langmuir : the ACS journal of surfaces and colloids* **2011,** *27*, 14317-14328.

(22) Keller, C. A.; Glasmästar, K.; Zhdanov, V. P.; Kasemo, B. Formation of Supported Membranes from Vesicles. *Physical Review Letters* **2000,** *84*, 5443-5446.

(23) Keller, C. A.; Kasemo, B. Surface specific kinetics of lipid vesicle adsorption measured with a quartz crystal microbalance. *Biophysical Journal* **1998,** *75*, 1397-1402.

(24) Reimhult, E.; Höök, F.; Kasemo, B. Intact Vesicle Adsorption and Supported Biomembrane Formation from Vesicles in Solution: Influence of Surface Chemistry, Vesicle Size, Temperature, and Osmotic Pressure†. *Langmuir : the ACS journal of surfaces and colloids* **2003,** *19*, 1681-1691.

(25) Johnson, J. M.; Ha, T.; Chu, S.; Boxer, S. G. Early steps of supported bilayer formation probed by single vesicle fluorescence assays. *Biophysical Journal* **2002,** *83*, 3371-3379.

(26) Hamai, C.; Yang, T. L.; Kataoka, S.; Cremer, P. S.; Musser, S. M. Effect of average phospholipid curvature on supported bilayer formation on glass by vesicle fusion. *Biophysical Journal* **2006,** *90*, 1241-1248.

(27) Hamai, C.; Cremer, P. S.; Musser, S. M. Single giant vesicle rupture events reveal multiple mechanisms of glass-supported bilayer formation. *Biophysical Journal* **2007,** *92*, 1988-1999.

(28) Richter, R.; Mukhopadhyay, A.; Brisson, A. Pathways of lipid vesicle deposition on solid surfaces: A combined QCM-D and AFM study. *Biophysical Journal* **2003,** *85*, 3035-3047.

(29) Richter, R. P.; Brisson, A. R. Following the formation of supported lipid bilayers on mica: A study combining AFM, QCM-D, and ellipsometry. *Biophysical Journal* **2005,** *88*, 3422-3433.

(30) Reviakine, I.; Brisson, A. Formation of supported phospholipid bilayers from unilamellar vesicles investigated by atomic force microscopy. *Langmuir : the ACS journal of surfaces and colloids* **2000,** *16*, 1806-1815.

(31) Richter, R. P.; Berat, R.; Brisson, A. R. Formation of solid-supported lipid bilayers: An integrated view. *Langmuir : the ACS journal of surfaces and colloids* **2006,** *22*, 3497-3505.

(32) Schonherr, H.; Johnson, J. M.; Lenz, P.; Frank, C. W.; Boxer, S. G. Vesicle adsorption and

lipid bilayer formation on glass studied by atomic force microscopy. *Langmuir : the ACS journal of surfaces and colloids* **2004,** *20*, 11600-11606.

(33) Weirich, K. L.; Israelachvili, J. N.; Fygenson, D. K. Bilayer Edges Catalyze Supported Lipid Bilayer Formation. *Biophysical Journal* **2010,** *98*, 85-92.

(34) Zhdanov, V. P.; Keller, C. A.; Glasmästar, K.; Kasemo, B. Simulation of adsorption kinetics of lipid vesicles. *The Journal of Chemical Physics* **2000,** *112*, 900-909.

(35) Plunkett, P.; Camley, B. A.; Weirich, K. L.; Israelachvili, J.; Atzberger, P. J. Simulation of edge facilitated adsorption and critical concentration induced rupture of vesicles at a surface. *Soft Matter* **2013,** *9*, 8420-8427.

(36) Gavutis, M.; Lata, S.; Piehler, J. Probing 2-dimensional protein-protein interactions on model membranes. *Nature protocols* **2006,** *1*, 2091-103.

(37) Hogbom, J. A. Aperture synthesis with a non-regular distribution of interferometer baselines. *Astronomy and Astrophysics Supplement Series* **1974,** *15* 417-26.

(38) Henriques, R.; Lelek, M.; Fornasiero, E. F.; Valtorta, F.; Zimmer, C.; Mhlanga, M. M. QuickPALM: 3D real-time photoactivation nanoscopy image processing in ImageJ. *Nature Methods* **2010,** *7*, 339-340.

(39) Woll, D.; Kolbl, C.; Stempfle, B.; Karrenbauer, A. A novel method for automatic single molecule tracking of blinking molecules at low intensities. *Physical Chemistry Chemical Physics* **2013,** *15*, 6196-6205.

(40) Holden, S. J.; Uphoff, S.; Hohlbein, J.; Yadin, D.; Le Reste, L.; Britton, O. J.; Kapanidis, A. N. Defining the Limits of Single-Molecule FRET Resolution in TIRF Microscopy. *Biophysical Journal* **2010,** *99*, 3102-3111.

(41) Rust, M. J.; Bates, M.; Zhuang, X. W. Sub-diffraction-limit imaging by stochastic optical

reconstruction microscopy (STORM). *Nature Methods* **2006,** *3*, 793-795.

(42) Huang, B.; Wang, W. Q.; Bates, M.; Zhuang, X. W. Three-dimensional super-resolution imaging by stochastic optical reconstruction microscopy. *Science* **2008,** *319*, 810-813.

(43) Mashanov, G. I.; Molloy, J. E. Automatic detection of single fluorophores in live cells. *Biophysical Journal* **2007,** *92*, 2199-2211.

(44) Ripley, B. D. Modeling spatial patterns. *Journal of the Royal Statistical Society Series B-Methodological* **1977,** *39*, 172-212.

(45) Goreaud, F.; Pelissier, R. On explicit formulas of edge effect correction for Ripley's K-function. *Journal of Vegetation Science* **1999,** *10*, 433-438.

(46) Getis, A.; Franklin, J. 2nd-order neighborhood analysis of mapped point patterns. *Ecology* **1987,** *68*, 473-477.

(47) Kiskowski, M. A.; Hancock, J. F.; Kenworthy, A. K. On the Use of Ripley's K-Function and Its Derivatives to Analyze Domain Size. *Biophysical Journal* **2009,** *97*, 1095-1103.

(48) Henriques, R.; Lelek, M.; Fornasiero, E. F.; Valtorta, F.; Zimmer, C.; Mhlanga, M. M. QuickPALM: 3D real-time photoactivation nanoscopy image processing in ImageJ. *Nature methods* **2010,** *7*, 339-340.

(49) Knoll, W.; Frank, C. W.; Heibel, C.; Naumann, R.; Offenhausser, A.; Ruhe, J.; Schmidt, E. K.; Shen, W. W.; Sinner, A. Functional tethered lipid bilayers. *Journal of biotechnology* **2000,** *74*, 137-158.

(50) Wagner, M. L.; Tamm, L. K. Tethered polymer-supported planar lipid bilayers for reconstitution of integral membrane proteins: silane-polyethyleneglycol-lipid as a cushion and covalent linker. *Biophys J* **2000,** *79*, 1400-1414.

(51) Wagner, M. L.; Tamm, L. K. Reconstituted syntaxin1a/SNAP25 interacts with negatively

charged lipids as measured by lateral diffusion in planar supported bilayers. *Biophys J* **2001,** *81*, 266-275.

(52) Waichman, S.; Bhagawati, M.; Podoplelova, Y.; Reichel, A.; Brunk, A.; Paterok, D.; Piehler, J. Functional Immobilization and Patterning of Proteins by an Enzymatic Transfer Reaction. *Analytical Chemistry* **2010,** *82*, 1478-1485.

(53) Wagner, M. L.; Tamm, L. K. Reconstituted syntaxin1A/SNAP25 interacts with negatively charged lipids as measured by lateral diffusion in planar supported bilayers. *Biophysical Journal* **2001,** *81*, 266-275.

(54) Wagner, M. L.; Tamm, L. K. Tethered polymer-supported planar lipid bilayers for reconstitution of integral membrane proteins: Silane-polyethyleneglycol-lipid as a cushion and covalent linker. *Biophysical Journal* **2000,** *79*, 1400-1414.

(55) Tanaka, M.; Tutus, M.; Kaufmann, S.; Rossetti, F. F.; Schneck, E.; Weiss, I. M. Native supported membranes on planar polymer supports and micro-particle supports. *Journal of Structural Biology* **2009,** *168*, 137-142.

(56) Sinner, E.-K.; Ritz, S.; Naumann, R.; Schiller, S.; Knoll, W. SELF-ASSEMBLED TETHERED BIMOLECULAR LIPID MEMBRANES. In *Advances in Clinical Chemistry, Vol 49*, Makowski, G. S., Ed., 2009; Vol. 49, pp 159-179.

(57) Sackmann, E.; Tanaka, M. Supported membranes on soft polymer cushions: fabrication, characterization and applications. *Trends in Biotechnology* **2000,** *18*, 58-64.

(58) Li, E.; Merzlyakov, M.; Lin, J.; Searson, P.; Hristova, K. Utility of surface-supported bilayers in studies of transmembrane helix dimerization. *Journal of Structural Biology* **2009,** *168*, 53-60.

(59) Knoll, W.; Frank, C. W.; Heibel, C.; Naumann, R.; Offenhausser, A.; Ruhe, J.; Schmidt, E.

K.; Shen, W. W.; Sinner, A. Functional tethered lipid bilayers. *Journal of biotechnology* **2000,** *74*, 137-58.

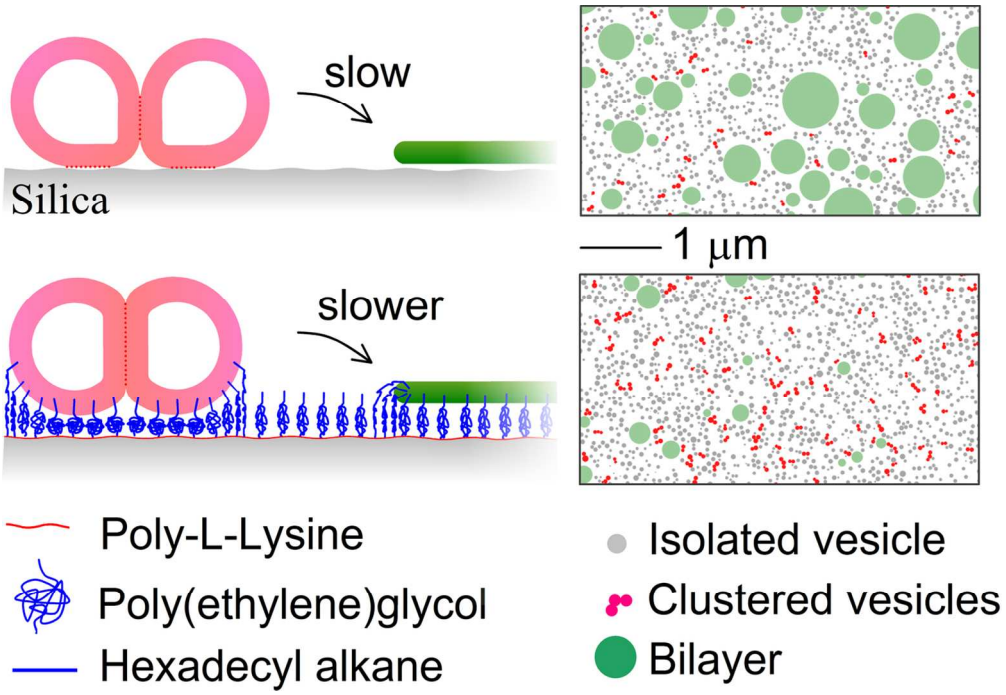

122x83mm (300 x 300 DPI)

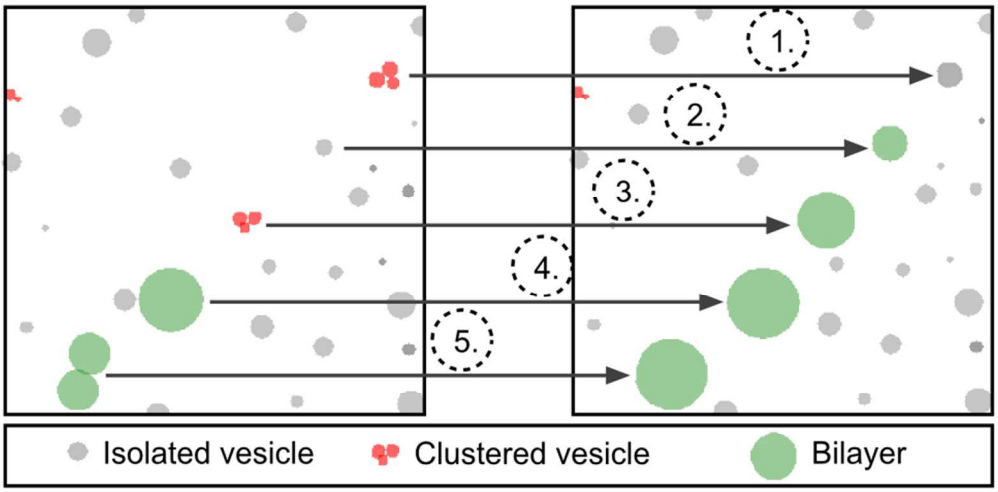

Scheme 1 Previously identified substrate-induced membrane remodelling pathways that see surface immobilized SUVs rupture or fuse: (1) vesicle-vesicle merger, 25 (2) isolated vesicle rupture, 9, 25 (3) vesicle induced vesicle rupture, 9, 25 (4) bilayer edge induced vesicle rupture 9, 27, 33 and (5) bilayer-bilayer merger 27
81x40mm (300 x 300 DPI)

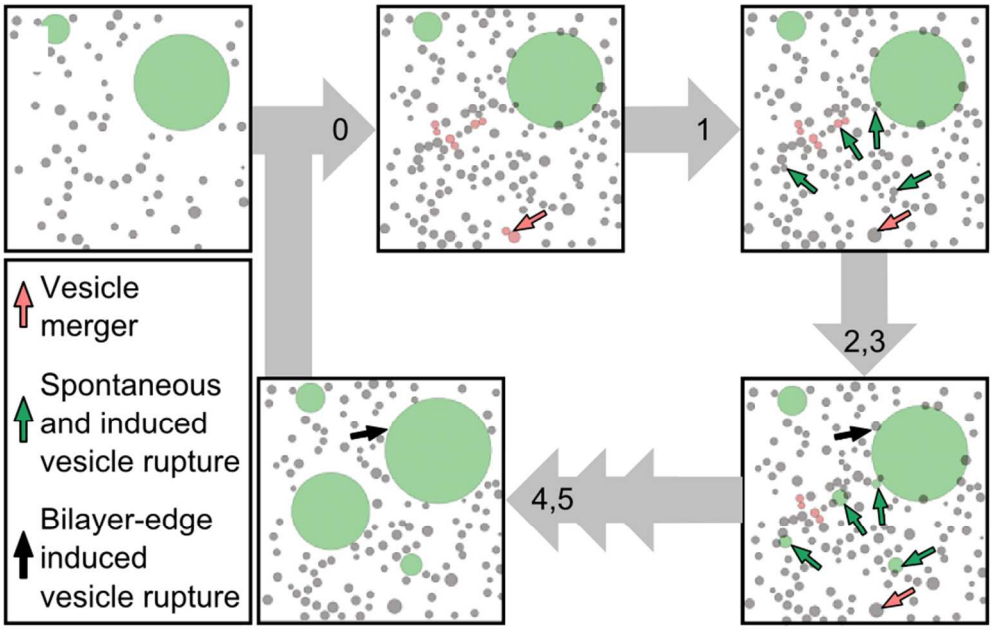

Scheme 2 Simulation stages: From an initial state (0) vesicles are deposited on the surface in accordance with the measured RIF trace at random locations outside the occluded area (i.e. not on top of a bilayer or a vesicle). (1) Vesicles in contact may merge with a probability PM. (2,3) Vesicles have a chance to rupture into bilayers: isolated vesicles with a probability P0; vesicles with N contacts with probability PN. (4,5) Bilayer edge induced vesicle rupture is carried out with a probability PR. Bilayer-bilayer merger always occurs to reflect the high reactivity of bilayer edges. The cycle is repeated every Δt (typically 100 ms). For a given input RIF time-trace and different values of PM, P0, PN and PR fluorescence traces for membrane merger and vesicle rupture are simulated and compared with the experimentally measured traces.
82x52mm (300 x 300 DPI)

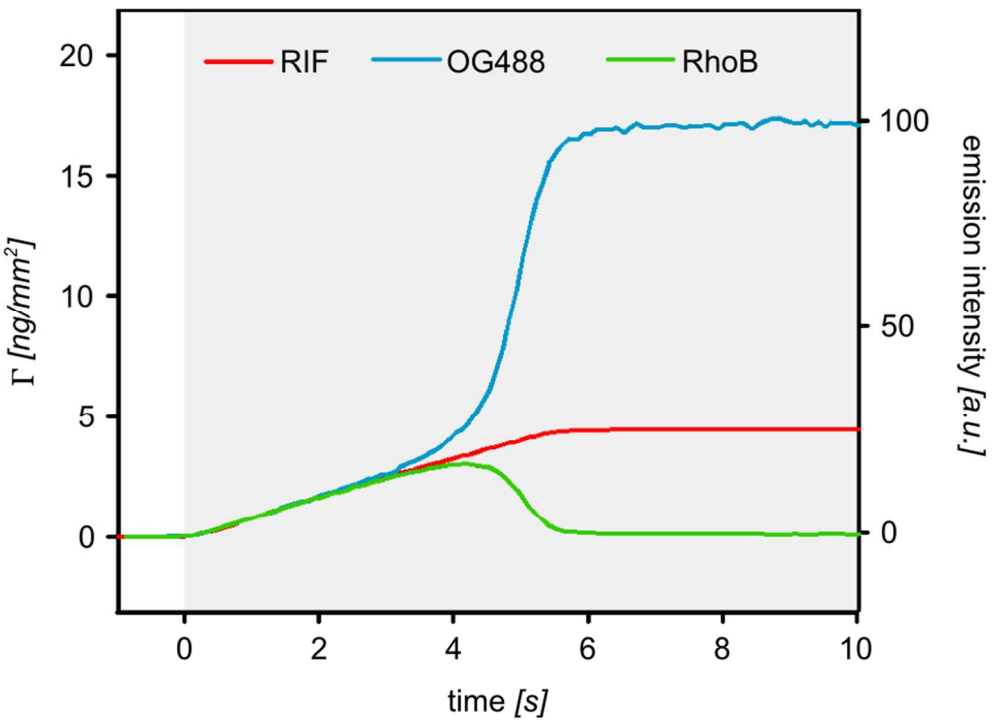

Figure 1 Vesicle binding to silica is diffusion rather than affinity controlled and vesicle rupture and membrane merger begins well before surface saturation: Simultaneous measurement of vesicle deposition (RIF trace, red), vesicle rupture (Oregon Green 488, blue) and membrane merger (Sulforhodamine, green). Injection period is marked with a grey background.
82x59mm (300 x 300 DPI)

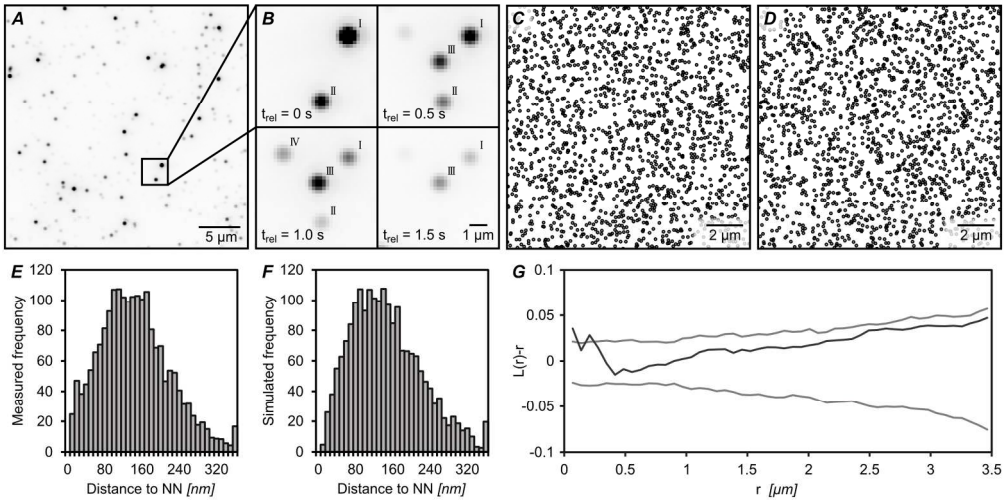

Figure 2: Super-resolution imaging shows random spatial distribution of surface bound vesicles: (A) A typical frame acquired using an objective coupled TIRFM with high laser power to ensure rapid photo bleaching. (B) 4 successive frames of the cropped area showing photo bleaching of the adhered vesicles and arrival of fresh vesicles. (C) Example location map of all vesicles deposited between 5-20% of full surface loading and (D) simulated random distribution for the same number of vesicles. Histograms showing distance of each vesicle to its nearest neighbour for (E) a measured vesicle location map, and (F) a simulated random distribution. (G) Comparison of measured vesicle distribution for the range of 5-20% of full surface loading (black line) to complete spatial randomness (CSR) using Ripley's K-function test. No deviation of the measured profiles outside the 99% confidence interval (generated from 500 simulations of random distributions; grey lines) indicates randomness at that length scale.
556x276mm (96 x 96 DPI)

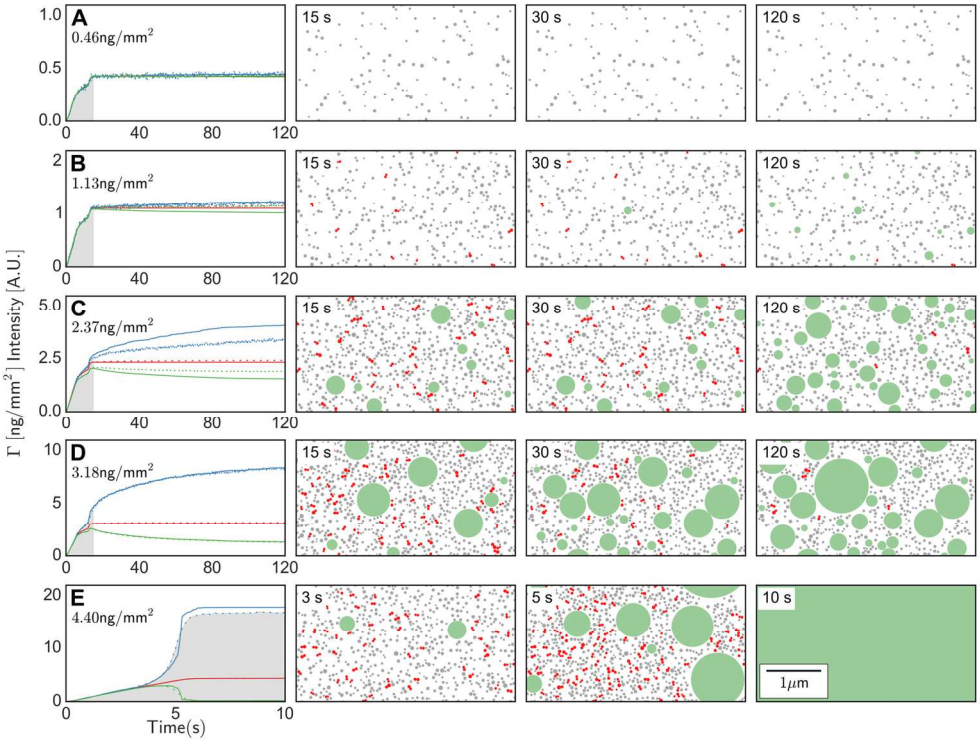

Figure 3 Measurements and simulations of surface loading dependent vesicle rupture and lipid mixing show rupture of clustered vesicles is the rate limiting step for SSB formation: Measured (dashed) and simulated (solid) RIF (red), RhoB (green) and OG488 (blue) traces for surface loadings of (A) 0.46, (B) 1.13, (C) 2.37, (D) 3.18, and (E) 4.4 ng.mm-2. Injection period is marked with a grey background. Images to the right show the simulated spatial distribution of isolated vesicles (grey), vesicles in contact with other vesicles (red) and bilayers (green) at different time points for the corresponding simulated fluorescence traces.
152x114mm (300 x 300 DPI)

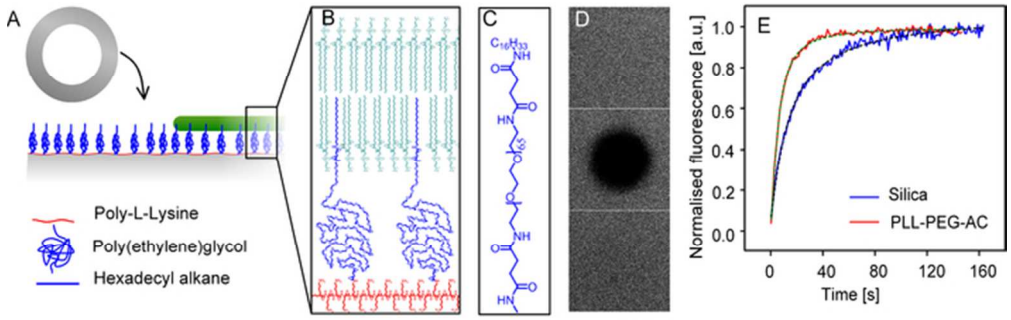

Figure 4 Vesicle deposition on PLL-PEG-AC leads to bilayer formation: (A) Surface architecture of silica coated with PLL-PEG-AC. (B) Chemical architecture of PLL-PEG-AC and SOPC bilayer (C) Chemical structure of PEG-AC attached to PLL. (D) Confocal laser scanning images showing fluorescence-recovery after photo-bleaching for a bilayer formed by SOPC vesicle doped with 0.2% OG488-DHPE on PLL-PEG-AC; first frame: immediately before photo-bleaching, second frame: immediately after photobleaching, third frame: 30 s post bleaching. (E) Normalised fluorescence from the bleached region demonstrating efficient recovery over time for silica (blue line) and PLL-PEG-AC (red line).
59x20mm (300 x 300 DPI)

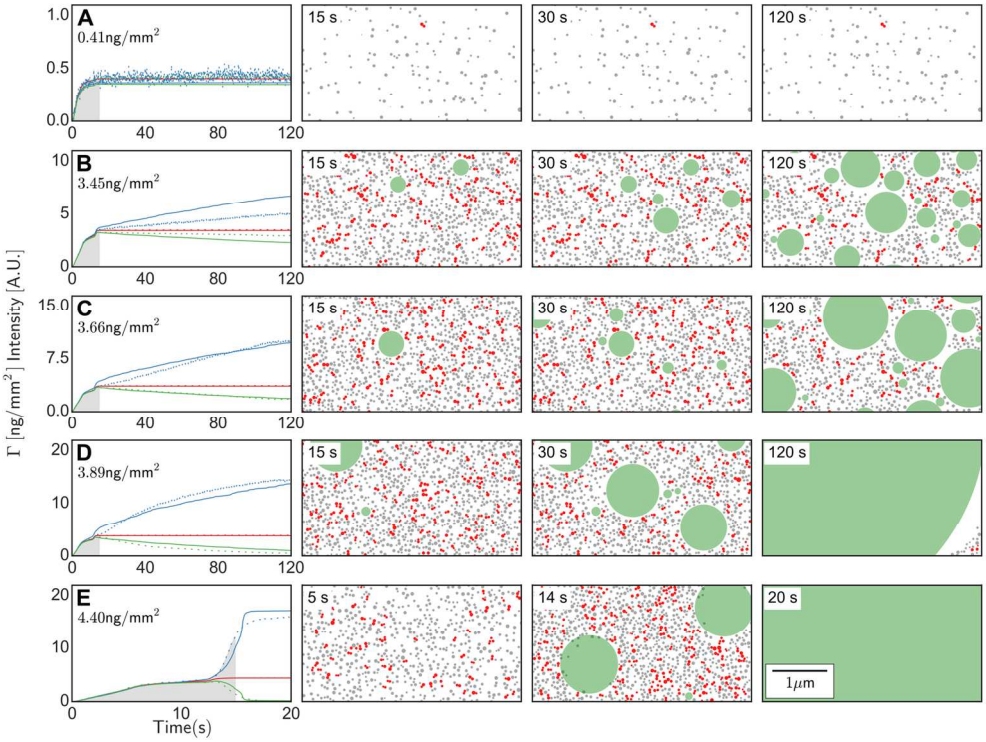

Figure 5 Measurements and simulations of surface loading dependent vesicle rupture and lipid mixing show rupture of clustered vesicles is the rate limiting step for PSB formation: Measured (dashed) and simulated (solid) traces for RIF (red), RhoB (green) and OG488 (blue) for surface loadings of (A) 0.41, (B) 3.45, (C) 3.66, (D) 3.89, and (E) 4.4 ng.mm-2. Injection period is marked with a grey background. Images to the right show the spatial distribution of isolated vesicles (grey), vesicles in contact with other vesicles (red) and bilayers (green) at different time points. Scale bar 1μm.
152x114mm (300 x 300 DPI)

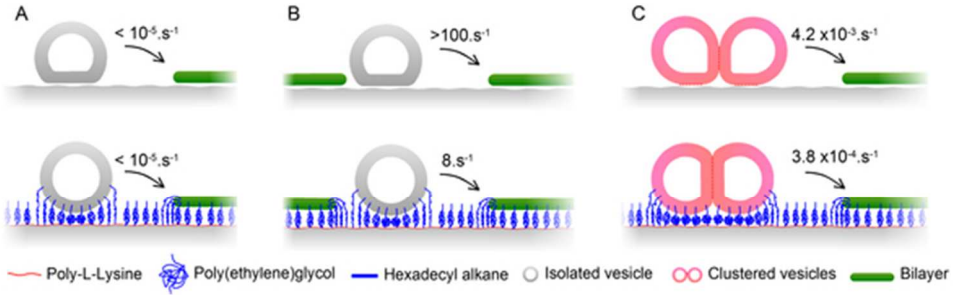

Scheme 3 Rate constants for a selection of vesicle remodelling paths on silica and silica coated with PLL-PEG-AC: A) rupture of individual vesicles to form isolated bilayer patches, B) Bilayer-edge induced assimilation of vesicles, C) rupture of binary vesicle cluster to form an isolated bilayer patch.
52x15mm (300 x 300 DPI)

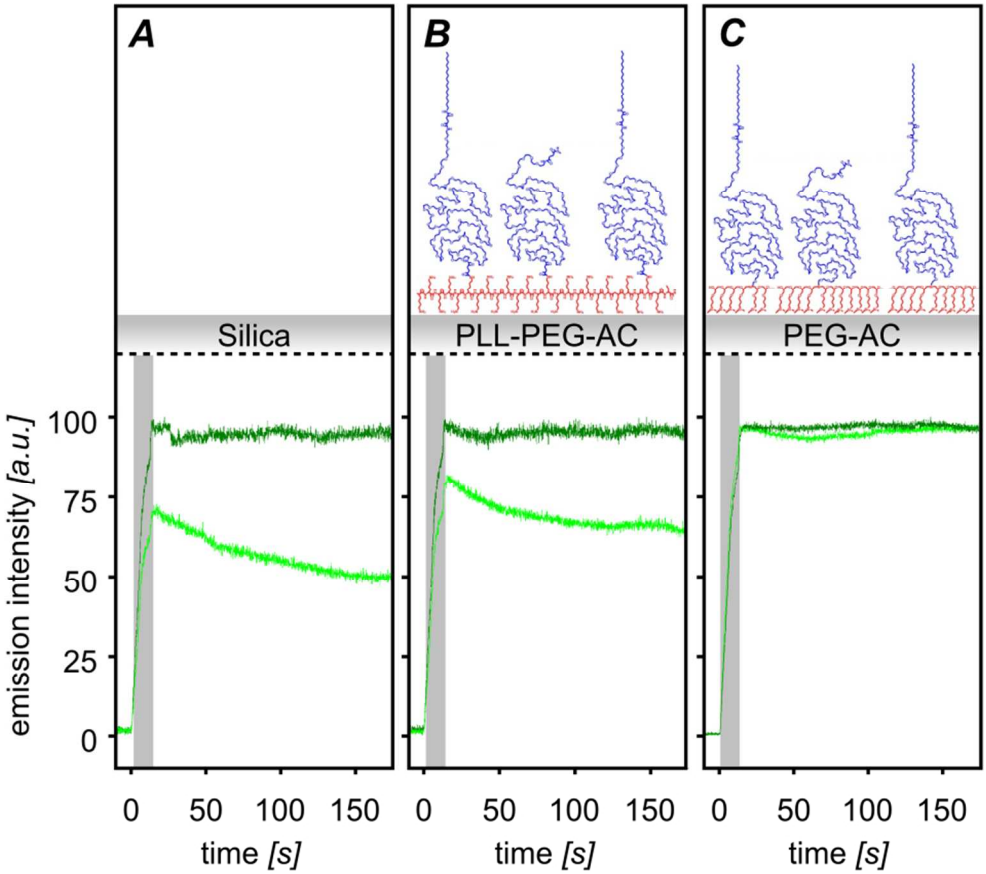

Figure 6 Increased rupture rates of pre-clustered vesicles: Normalized RhoB trace for cross-linked (light green) and un-cross-linked (dark green) vesicles on (A) silica, (B) PLL-PEG-AC and (C) PEG-AC.18 Injection periods are marked with a grey background. Top panels show the surface-types.
343x300mm (72 x 72 DPI)

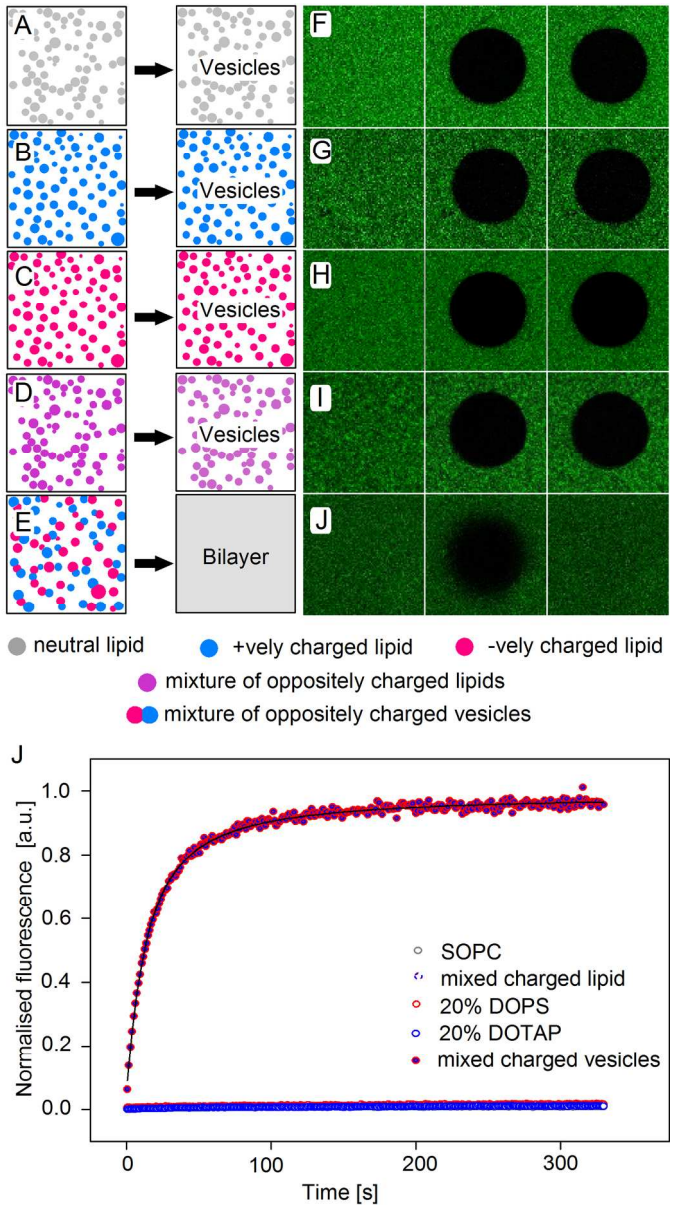

Figure 7 Promoting bilayer formation via electrostatically induced clustering: Schematic representation of lateral distribution of (A) neutral, (B) positively, (C) negatively and (D) a mixture of positively and negatively charged lipids and (E) a mixture of positively and negatively charged vesicles on a neutral PEG-AC surface. Frames before bleaching, immediately after bleaching and 30 s post bleaching for surface adsorbed (F) SOPC, (G) 20% DOPS+ 80% SOPC, (H) 20% DOTAP + 80% SOPC (I) 10% DOTAP + 10% DOPS + 80% SOPC and a (J) 1:1 mixture of 20% DOPS and 20% DOTAP vesicles. (K) Intergrated fluorescence from the bleached spot as a function time for SOPC (black open circle), 20% DOPS+ 80% SOPC (red open circle), 20% DOTAP + 80% SOPC (blue open circle), 10% DOTAP + 10% DOPS + 80% SOPC (red and blue open circle) and a 1:1 mixture of 20% DOPS and 20% DOTAP vesicles (red and blue circle).
144x254mm (300 x 300 DPI)